Chapter 11
Future Opportunities

Abstract In this chapter we present an overview of the prospects of forthcoming experimental and theoretical advances in areas like the use of femtosecond X-ray pulses from a free electron laser for ultrashort imaging of biological materials without causing sample damage, X-ray scattering interferometry, application of terahertz radiation, frequency combs for broadband high-precision spectroscopy, coherently controlling biochemical reactions and explorations of biological entities beyond the quantum limit.

11.1 Outlook

Experimental as well as theoretical methods developed in fields of research as diverse as femtochemistry, semiconductor physics, statistical mechanics and quantum information processing, among others, are likely to open up new directions of research and development in ultrafast biophotonics. For instance, single-molecule studies (Chap. 4) have already started providing remarkable new insights into functions of biological systems [1, 2]. These phenomena were previously hidden in the ensemble average common to almost all earlier studies. Investigations of quantum-dynamical phenomena at the single-molecule level are very challenging because of the ultrashort timescales involved. However, recent observations of vibrational coherence in individual molecules at ambient temperatures by means of a phase-locked spontaneous fluorescence technique auger well for future developments [2]. Application of this technique to detect electronic coherence in photosynthetic complexes (Chaps. 4 and 7) and photoreceptors (Chap. 8) may provide important new insights into quantum energy flow in biology. In the following we present an overview of some other topics which, in the authors' opinions, are likely to be vigorously pursued in the coming years. The prognosis is extremely good for qualitative leaps to be attained vis-a-vis development of new insights into biophotonics.

P. Vasa and D. Mathur, *Ultrafast Biophotonics*, Biological and Medical Physics, Biomedical Engineering, DOI 10.1007/978-3-319-39614-9_11

11.2 Femtosecond X-Ray Imaging

The advent of femtosecond-long hard X-rays from free electron laser (FEL) facilities, such as the Linac Coherent Light Source (LCLS) in Stanford, FLASH (Free electron LASer in Hamburg), and SACLA (the SPring-8 Angstrom Compact Free Electron Laser) in Aioi is beginning an entirely new era for biological imaging. The intense, ultrashort pulses of X-rays that are available from such free electron laser sources now permit diffraction imaging to be obtained of very small biological structures on timescales that are too short for radiation-induced damage to occur. Conventionally, X-rays from synchrotron storage rings have, over the years, provided invaluable structural information leading to new insights into a whole gamut of biological materials. However, all such measurements have required the sample that is to be probed to be in the form of reasonably large crystals: millions of molecules need to be aligned in a crystal in order for experimentalists to obtain sufficient X-ray signal to produce sensible diffraction patterns. However, there are many classes of biological materials that "refuse" to crystallize. One example of many are the human cell membrane proteins, of critical importance as drug targets. In a new generation of experiments that are beginning to be reported from free electron lasers, structure determinations have now begun to be made of macromolecular material in *nanocrystalline* form; such materials have, thus far, proved difficult to grow as large crystals. As discussed in the following, ultrashort beams of X-rays now enable millions of diffraction patterns to be obtained from an intersecting stream of nanocrystals. Amongst the first biological entities to be studied in this fashion was the membrane protein, photosystem I, in the form of a stream of nanocrystals of dimensions in the range ~200–2000 nm.

It is known that membrane proteins play a critically important role in determining the way cells and viruses function. However, insights into their structure and the dynamics that drive their functioning continue to remain elusive. Photosystem I is one of the largest of membrane protein complexes (it has a molecular mass of 1 MDa; it comprises as many as three dozen proteins and 381 cofactors). Acting as a biosolar energy converter, photosystem I is at the heart of the process of oxygenic photosynthesis (Chap. 7). One of the difficulties of gaining information about this membrane protein has been its intransigence in producing large enough crystals for experiments to be carried out. Crystals of photosystem I are expected to possess symmetry of space group $P63$, with unit-cell parameters $a = b = 281$ Å and $c = 165$ Å; typically, each crystal comprises as much as 78 % solvent by volume.

The major factor that has, for a long time, limited the attainable resolution in biological imaging has been radiation damage when energetic electrons or X-rays are used [3]. The ultrafast X-ray pulses that are becoming available from FELs circumvent radiation damage by using single X-ray pulses that are of such short duration (10 fs, and even lower) that the pulse has disappeared well before there is the possibility of any damage to the irradiated sample manifesting itself [4]. This was first demonstrated at experiments carried out at FLASH: "diffraction before destruction" at resolution lengths down to 60 Å was demonstrated on samples fixed on silicon nitride films [5]. Subsequent experiments on photosystem I, carried out

at LCLS, demonstrated that the concept of "diffraction before destruction" can also be operative at sub-nm resolution. This enabled the establishment of a protocol for structure determination based on accumulating X-ray diffraction data from a sample that takes the form of a stream of photosystem I nanocrystals [6]. It is interesting to note that these nanocrystals were no larger than 300 nm along their edge, that is equivalent to only 10 unit cells!

For those biological entities that are intrinsically non-crystalline, it has been possible to use X-ray pulses from an FEL to obtain diffraction images of materials like the mimivirus by injecting a beam of cooled mimivirus particles into the X-ray beam [7]. Mimivirus is a microbe-mimicking virus, which is among the largest of known viruses [8]; its large size (about 0.75 μm in diameter) makes it more or less comparable to the size of the smallest living cells. This makes it too large for a full three-dimensional reconstruction by means of conventional cryo-electron microscopy. Results of calculations carried out concomitantly with the FEL experiments offered indications that the energy deposited into the virus by the X-ray pulse heated the virus to a temperature of over 100,000 K after the pulse has left the sample, once again demonstrating the efficacy of extremely bright, coherent X-ray pulses being so ultrashort that key damage processes simply do not have time to occur before a diffraction pattern is recorded from a large macromolecule, a cell, or even a virus prior to it becoming plasma and exploding.

As in the case of experiments with photosystem I there was no measurable deleterious effects of the X-rays on the sample. It has been conjectured that X-ray pulses from the FEL induce hydrodynamic explosion of μm-sized objects such that the outside portion of the irradiated sample "burns" first, with heat being transported inwards, rarefying and destroying outer contours first. As a consequence, trapped electrons move inwards into the sample, neutralizing the core which has become positively charged. The inward movement of electrons leads to a positively charged outer layer, which then peels off on picosecond timescales [5].

It is anticipated that considerable progress will be made in the coming years in utilizing ultrafast X-rays from FEL sources in order to determine in vivo crystal structures. Both prokaryotic as well as eukaryotic cells contain proteins in microcrystalline form. Such macromolecules have, almost always hitherto, been studied by first biochemically extracting them from the cells and then recrystallizing them in vitro for conventional X-ray crystallography, usually with synchrotron sources. Cell biologists have long pondered over whether the in vitro macromolecular structures that are experimentally determined fully resemble the real in vivo structures. Femtosecond crystallography that is now becoming accessible at FEL sources makes the question answerable, and the earliest experiments addressing this issue have begun to be performed [9]. Experiments have been conducted at LCLS on a toxin (Cry3A) that is produced by *Bacillus thuringiensis* (Bt) and stored in bacterial cells as naturally-formed microcrystals. The measurements involved the streaming of whole Bt cells into the X-ray beam from the LCLS FEL. The photon energy in the beam was ∼9 keV, corresponding to ∼1.5 Å, with a pulse duration of 40 fs, a repetition rate of 120 Hz, and a flux of $\sim 10^{11}$ photons per pulse. The naturally grown crystals of Cry3A in Bt cells were injected into the path of the X-ray beam; they traversed a distance of

~200 μm, taking about 3.0–7.5 μs to reach the X-ray beam. The conjecture was that even if this time is sufficient for the cell walls to rupture—an unlikely scenario—it is still not sufficient for the Cry3A crystals to dislodge from within the Bt cells; there would most certainly not be enough time for the toxin molecules of the cellular crystals dislodged from Bt to recrystallize into some different form. As it turns out in this particular case, the structure that was determined for the in vivo crystals was essentially the same as that for in vitro crystals. Structure of in vivo crystals have also been determined in the case of glycosylated cathepsin from *Trypanosoma brucei* (TbCatB) [10], knockdown of which has been shown to be lethal to the parasite responsible for sleeping sickness that affects several million people across Central Africa. The enormous potential that femtosecond X-ray diffraction offers for cell biology cannot be understated. As already noted, considerable progress is anticipated in this emerging area of ultrafast cell biophotonics, perhaps even the prospect of addressing one of the central themes of cell biology, that cellular components are structured: cells are far more than floppy bags of freely moving molecules.

So, how are femtosecond X-ray pulses generated in an FEL? Unlike conventional femtosecond laser systems that rely on the light-emitting properties of materials for lasing, the heart of an FEL lies in producing high energy electrons and manipulating their trajectories such that the light they emit is at X-ray wavelengths (1–0.1 nm). As it is primarily free electrons from ionization of atoms that are the progenitors of the X-rays, this relatively recent entrant into the world of lasers is referred to as an X-ray free electron laser (XFEL). Figure 11.1 is a schematic depiction of how electrons are produced, by irradiating a photocathode with an intense femtosecond laser beam and, subsequently, how they are accelerated and their trajectories manipulated by means of an undulator so as to produce energetic photons.

The fast electrons pass through the undulator in an uncoordinated manner; consequently, the light that they emit is incoherent. The strategy employed in an XFEL uses

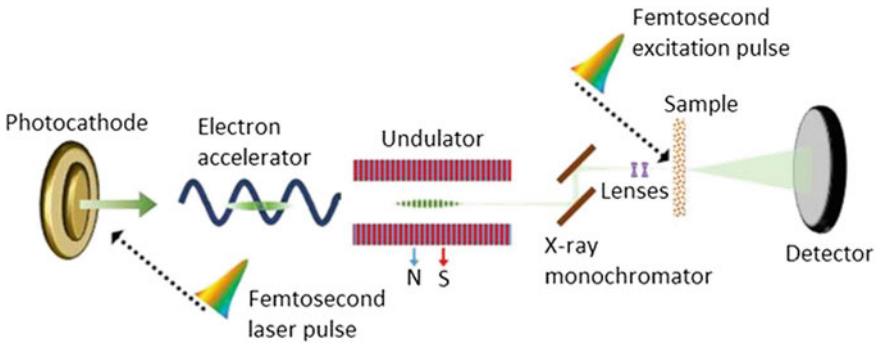

Fig. 11.1 Schematic depiction of how ultrafast X-ray pulses are generated in a free electron laser. An intense femtosecond laser irradiates a photocathode. The emitted electrons are accelerated through an undulator—a region of alternating magnetic fields comprising a series of magnets with North-South...SN...NS...SN configuration. The ensuing acceleration results in formation of ultrashort X-ray pulses which are made to impinge on a biosample. This sample can be simultaneously excited by a second femtosecond laser beam and the X-rays interrogate the excited biosample on ultrashort timescales

the concept of self-amplified spontaneous emission (SASE). Instead of the energetic electrons oscillating through the resonator many times so as to increase the effective interaction length (as in a conventional laser cavity), in SASE the undulator is timed such that light emitted by a bunch of electrons interferes with the preceding electron bunch. This photon-electron interaction results in temporal and spatial modulation of electron density, generating spectrally narrow emission with relatively long coherence length. SASE has been successfully employed in all XFEL facilities to create useable beams of coherent X-rays.

Although the use of femtosecond-duration, coherent X-ray beams from XFEL facilities are opening new vistas for diffraction imaging that unveils the internal structure of cells and organelles, it is pertinent to draw brief attention to on-going experimental difficulties that still need to be resolved. One concerns the attainable spatial resolution: although very good, it is, nevertheless, limited to a few tens of nanometers. This is a consequence of the poor scattering power of most biological samples and, hence, the continuing challenge for experimentalists is to devise new methodologies that will help recover correct phase information from measured diffraction images that inevitably possess low signal-to-noise ratio and from lowest-resolution data.

Some novel approaches are beginning to be explored in attempts to enhance the attainable spatial resolution by (i) seeking to enhance diffraction signals and (ii) by more robust phasing. The weak diffraction signals that emanate from most biological objects have recently been sought to be enhanced by interference with strong diffracting waves from dispersed colloidal gold particles that are embedded within the biological sample of interest. X-ray imaging is carried out of these Au-particles and the biological object of interest together [11]. Interference occurs between the strong diffraction waves emanating from the Au-particles on the one hand and the much weaker diffraction waves from the biological object on the other. Such interference is being utilized to enhance the signals from the biological object to a much more detectable level by the process of coherent amplification (see Sect. 11.3). Experimentally, the easily-observed positions on the detector of the Au-particles, as determined by conventional Patterson analysis [11], serve as the initial phase. As Au-particles are relatively unreactive, this approach is likely to prove to be compatible with the X-ray imaging of a wide variety of biological objects under physiologically-relevant conditions; early demonstrations from experimental images obtained using SACLA appear to testify to this [12].

The next major XFEL facility is expected to be the European XFEL, the precursor of which is FLASH. Table 11.1 summarizes some of the key attributes of this next-generation XFEL and compares it with the attributes currently exhibited by SACLA and LCLS.

It is also of interest to make comparison of X-ray photons from an FEL with photons from femtosecond infrared lasers. As the ponderomotive energy (Chap. 2) gained by ionized electrons depends on the inverse square root of photon energy, it is clear that processes like above-threshold ionization, rescattering, and its consequences, such as high harmonic generation, that are readily encountered in femtosecond duration pulses from a conventional laser (Chap. 2) are essentially "switched off"

Table 11.1 Comparison of the attributes of XFEL facilities: SACLA in Aioi, LCLS in Stanford, and the forthcoming European XFEL in Hamburg

Property	SACLA	LCLS	Euro-XFEL
Commissioning date	2011	2009	2017
Repetition rate	60 Hz	120 Hz	27 kHz
Shortest wavelength	0.08 nm	0.15 nm	0.05 nm
Max. electron energy	8 GeV	14.3 GeV	17.5 GeV
Length	0.75 km	3 km	3.4 km
No. of undulators	3	1	3–5
Peak brilliance[a]	1×10^{33}	2×10^{33}	5×10^{33}
Average brilliance[a]	1.5×10^{23}	2.4×10^{22}	1.6×10^{25}

[a] In units of photons/s/mm^2/mrad^2/0.1 % bandwidth

in the case of photons from an FEL. For 92.5 eV photons that are readily available from, for instance, FLASH, at an intensity of 10 TW cm^{-2}, the corresponding photon wavelength is 13.4 nm and, hence, the ponderomotive potential is only 160 meV. In contrast, with a photon pulses of similar peak intensity from a Ti:sapphire laser, where the photon energy is 1.55 eV, the ponderomotive potential is a massive 600 eV. For Xe atoms—whose first ionization energy is 12.13 eV, the FLASH parameters yield a Keldysh parameter, γ, of 8.7, well into the multiphoton ionization regime. Hence, FLASH (as well as LCLS and SACLA) photons of 10 TW cm^{-2} peak intensity will not induce tunnel ionization while with photon pulses of the same peak intensity from a Ti:sapphire laser the ionization of Xe will be almost entirely due to tunneling.

11.3 X-Ray Scattering Interferometry and Molecular Rulers

Imaging methodologies in cell biology ultimately require both ultrafast time resolution and atomic-scale spatial resolution so that structural changes may be observed in an individual biomolecule [4, 13–16]. In the previous section, we have discussed the ultrafast pulsed X-ray source—the XFEL—which can provide the required time resolution. In the visible range, in vivo observations have significantly progressed due to remarkable developments in labeling and single-molecule fluorescence techniques [17, 18]. Appropriate labeling in single-molecule fluorescence measurements now succeeds in providing positional information with an accuracy of $\sim \frac{\lambda}{100}$, far better than the optical diffraction limit $\sim \frac{\lambda}{2}$. It would be desirable to achieve similar $\sim \frac{\lambda}{100}$, picometer-scale resolution [19, 20] in X-ray imaging for determining structures of biomolecules and, indeed, for dynamical studies.

The distances between different molecules or moieties in a given macromolecule are closely related to its 3D structure. Hence, for a macromolecule with a dynamic

conformation, distributions of distances between many different pairs of molecules or moieties can, in conjunction with a suitable theoretical model, help define the structural dynamics. Thus, in principle, the separation between two points—a "molecular ruler"—may be sufficient to experimentally deduce the molecular structure [21–23]. Though this is a promising approach, most existing rulers are sensitive only to relative changes in distances. They do not provide absolute distances; nor do they provide accurate enough occupancy distributions, particularly for a complex system in which multiple distances (or conformations) coexist. These limitations arise from (i) averaging of signals over a finite time, (ii) complex nonlinear and non-unique mapping between the observed signal and the molecular dynamics, and (iii) possible contributions to the observed signal from other parameters apart from distance. These limitations result in the lack of distance calibration on an absolute scale, preventing quantitative comparison of experimental results with those obtained from computational models [21–23].

Small-angle X-ray scattering interferometry address these issues and provides instantaneous and high-precision distance information that enables precise determination of macromolecular structures [21–23]. As in the case of fluorescence tagging [17, 18], biomolecules and proteins, for example DNA, are tagged with gold nanocrystals. Two gold nanocrystal probes are attached to two specific locations in a macromolecule [Fig. 11.2 (top)], and the mutual interference in the X-ray scattering

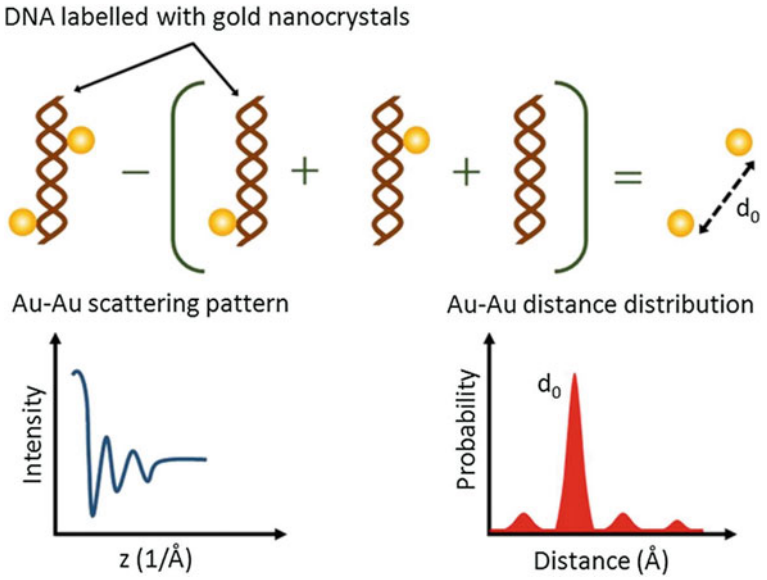

Fig. 11.2 Schematic of X-ray scattering interferometry and a "molecular ruler". A double helix DNA is labeled with a gold nanocrystal on each of the two DNA strands (*top*). The X-ray interference pattern, on Fourier transforming after subtracting the scattering signals from individual gold nanocrystals and the DNA molecule, yields information about the separation between the two nanocrystals (*bottom*)

of gold nanocystals is measured. As the scattering from gold nanocystals is much stronger than from organic molecules, due to the higher atomic number of gold and because the scattering is "instantaneous" compared to the slow atomic motions of the molecule, the interference pattern needs a much shorter time to record. Moreover, it provides precise information about the relative distance between the two nanocrystals. Fourier transforming the recorded interference pattern after necessary data processing (Fig. 11.2) directly provides an un-averaged snapshot of intramolecular distance between the gold probes, a structural measure of the thermodynamic landscape of conformational states. A major advantage of this technique is that data analysis is totally model-independent and does not require a priori knowledge (or conjecture) about the structure [21–23].

X-ray scattering interferometry on DNA double helices has been reported in which gold nanocrystal probes were placed at 18 different pairs of positions [21–23]. Distance distributions were measured to determine structural values for DNA helices in solution for comparison with other measurements and theoretical models. The results highlighted the limitations of the prevailing understanding that DNA behaves like a stiff elastic rod with respect to inherently ubiquitous mechanical deformations. Experimental investigations have revealed that in the absence of applied tension, DNA is at least one order of magnitude softer than indicated by single-molecule stretching experiments. Results have also shown a quadratic dependence between the end-to-end length in contrast to the linear dependence predicted by the conventional elastic rod model, suggesting more flexibility, occurrence of stretching over more than two turns of the double helix, and the possibility of long-range allosteric communication through the DNA structure [21–23]. Using similar labeling and X-ray tracking techniques, picometer-scale ($\sim\frac{\lambda}{100}$) Brownian and rotating motions of individual DNA molecules tightly linked to gold nanocrystals have also been reported [19]. The approach of labeling biomolecules with gold nanostructures and of tracking their scattering and/or interference patterns may, in coming years, also be extended to pulsed electron probes (Chap. 3) to develop a laboratory-scale time-resolved single-molecule detection system [20].

Coherent X-ray diffraction microscopy is another lens-less, phase-contrast imaging technique with high image contrast; it is label-free and can be used to investigate single cell organelles [14, 24–26]. Although well established techniques of electron tomography have allowed intensive study of the 3D structure of cellular organelles, they have proved to be difficult to apply to thick samples. X-ray probes can overcome these limitation without compromising on spatial resolution [25, 27–29].

Coherent X-ray diffraction occurs when a sample is illuminated with a well-defined wavefront. Upon encountering the scatterer, the phase-sensitive wavefront undergoes changes which can be utilized for microscopy. The coherently diffracted wavefront is related to the sample electron-density map by Fourier transform, but the phase of the diffracted wave is not directly measurable unless more complex interferometric techniques are employed. Moreover, phase information has to be retrieved for complete 3D reconstruction of the image. As already noted, coherent X-ray diffraction microscopy provides phase contrast information without using lenses or sample tagging [25, 30]. Thus, as in optical microscopy, it is superior to

conventional absorption contrast imaging X-ray microscopy [28, 29], particularly for transparent objects like human chromosomes and DNA [25, 31]. Being sensitive, it also offers advantages in terms of lower radiation dose and better signal-to-noise ratio (faster data collection) and higher image contrast, even in an aqueous environment. Reconstructed 3D images of a thick biological sample—an unstained human chromosome—have successfully reproduced an axial structure which other microscopic methods have been unable to visualize without staining [25]. The concept of coherent X-ray diffraction can be further extended to perform Talbot interferometry using a pair of diffraction gratings [32–34]. In this case the phase object is placed in front of one of the gratings and its structural information is obtained by analyzing the deformation of the fringe pattern. Using this technique, in situ properties of transparent biological specimens like eye lenses have been measured [32]. The eye lens, a major ocular component, has a gradient refractive index. The refractive index variations across the lens are dependent on the distributions and concentrations of various proteins and, consequently, of various electron density patterns. The interferograms map these variations and help reveal previously undetected conformations which might be linked to various developmental stages [32].

Though most of these techniques currently employ a continuous wave X-ray source, they can all be adapted for use with ultrafast pulsed X-ray and/or electron sources, which will enable them to simultaneously provide high spatial as well as temporal resolution. These techniques will then be able to shed light in hitherto unexplored directions in ultrafast biophotonics by correlating structures to mechanisms and functionalities of biomolecules and proteins.

11.4 Terahertz Spectroscopic Probes

Lab-on-a-chip DNA analyzers, DNA biosensors, and gene chips constitute contemporary techniques that continue to revolutionize genetic diagnostics. They mostly identify polynucleotide sequences by detecting the binding of unidentified DNA molecules to single-stranded oligo- or poly-nucleotide DNA of known base sequence. The unidentified DNA are the “target” while molecules with known sequences are the “probe”, and the basis of these techniques is the fact that binding of target to probe molecules is most likely to occur when they possess complementary base sequences. Such binding is referred to in the literature as “hybridization” and its detection currently relies on fluorescent labelling (and sensitive optical detection) of molecules of target DNA [35].

It has long been accepted that such labeling can often be accompanied by certain deficiencies, such as the fluorescence efficiency showing dependency on the binding site, and fluorescence yields being variable [36, 37]. From an operational point of view, labelling often appears to be a step that is unwanted by practicing biologists in that it appears to introduce complications to the analytical procedure for gene detection. Consequently, it is not surprising that there has long been an interest in

seeking an analytical technique that does away with labelling and it is in this context that there is contemporary interest in exploring terahertz (THz) methods.

THz radiation covers the part of the electromagnetic spectrum that spans the frequency range from about 0.1–10 THz. This range is especially appropriate for probing rovibrational excitation in molecules, both neutral and in ionized form, as well as localized vibrations that often accompany conformational changes in DNA. THz imaging offers several advantages that optical, nuclear magnetic resonance and X-ray methods do not, especially relating to conformational information about biomolecules in cells and tissues and how such changes might relate to biological functions [38]. One shortcoming of THz radiation in the context of biology is its very strong absorption by water, a medium in which most biological entities are immersed. Consequently, most contemporary diagnostic work that employs THz radiation has been carried out on dry samples, often in powder or thin film form. Studies of THz absorption have been reported on some proteins, nucleic acids, and tissues [39–44]. Very recently, time-domain spectroscopy in the THz region has begun to be successfully applied to enable studies to be carried out on biological samples in aqueous media [45]. Label-free detection of single-base mutations on oligonucleotides in aqueous solutions has been reported [45] in which a Ti:sapphire laser is utilized to produce sub-100 fs pulses that irradiate an InAs emitter of THz radiation. After passing through DNA molecules in aqueous phase, the THz field is detected using electro-optical sampling with a ZnTe crystal. Such experiments can be conducted at room temperature but stringent humidity control is mandatory (typically, relative humidity levels need to be kept below about 5 %). As can be seen in Fig. 11.3, observable changes in absorption spectra that can be ascribable

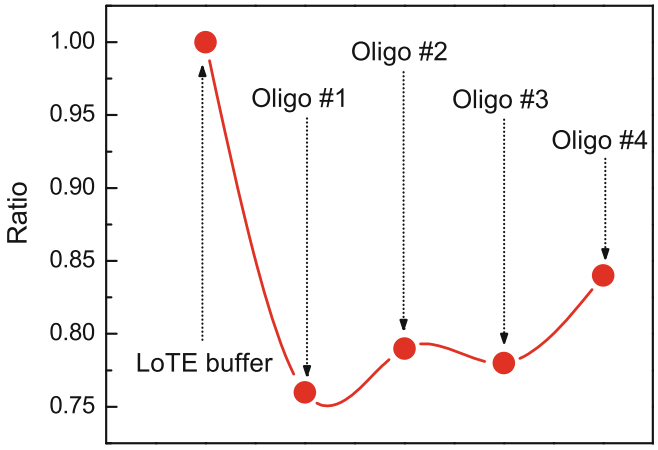

Fig. 11.3 Ratio of the THz signal being transmitted through neat LoTE buffer and LoTE buffer containing different oligonucleotides, Oligo #1–Oligo #4, based on measurements conducted by Tang et al. [45]. Peaks in the THz transmission function for neat buffer and oligonucleotides occur at 0.59–0.88 THz and the ratio that is plotted is the transmitted signal intensity: I at 0.88 THz/I at 0.59 THz

to single-base mutations have been convincingly demonstrated over the frequency range 0.2–2.6 THz [45].

The oligonucleotide sequences with single-base mutations referred to in Fig. 11.3 are as follows:

Oligo #1: TGGAGCTGGT***G***GCGTAGGCA;
Oligo #2: TGGAGCTGGT***C***GCGTAGGCA;
Oligo #3: TGGAGCTGGT***T***GCGTAGGCA; and
Oligo #4: TGGAGCTGGT***A***GCGTAGGCA.

The bold, italic letter in each oligonucleotide delineates the different bases. As is seen, single-base mutations give rise to (i) significantly lower THz transmission when compared to the neat buffer solution and (ii) the four oligonucleotides exhibit different absorption spectra, at least over the frequency range 0.2–2.6 THz. The relative changes in absorption peaks hold much promise for useful applications in future for THz spectroscopic methods of detection, in label-free fashion of single-base mutations.

11.5 Frequency Comb Fourier Transform Spectroscopy

Along with THz, the mid-infrared spectral region of 2–20 μm (500–5000 cm^{-1}) is a domain of very considerable interest in biophotonics because a large number of biomolecules exhibit strong characteristic vibrational transitions in this spectral range. Consequently, mid-infrared spectroscopy has proved to be a powerful tool for understanding the molecular structure governing microscopic mechanisms, and for performing non-intrusive diagnostics of composite biological systems [46, 47]. The low Rayleigh scattering losses in this spectral range are advantageous for tomography and imaging in turbid biological media. Fourier Transform Infrared (FTIR) Spectroscopy has emerged as one of the major tools for biophotonic and biomedical applications and is making significant contributions in clinical evaluation by providing molecular-level information that allows investigation of functional groups, bonding types, molecular conformations and surrounding environment. Research has been carried out on a number of natural tissues using FTIR spectroscopy because it is a relatively simple, reproducible, and nondestructive technique requiring only a small amount of sample with minimum preparation time [46–48].

However, identifying multiple, and possibly unknown, biomolecules requires a detailed spectroscopic analysis over a broad spectral bandwidth with high spectral resolution. A broad frequency "comb" comprising a series of discrete, equally spaced frequencies might prove to be an ideal light source for such applications [46, 49–55]. Laser frequency combs are coherent light sources that emit a broad spectrum of discrete, evenly-spaced narrow lines whose absolute frequency is stabilized and measured to within the accuracy of an atomic clock without the need to employ a conventional dispersive element-based spectrometer. They can be generated by a number of mechanisms, including amplitude modulation of a continuous wave

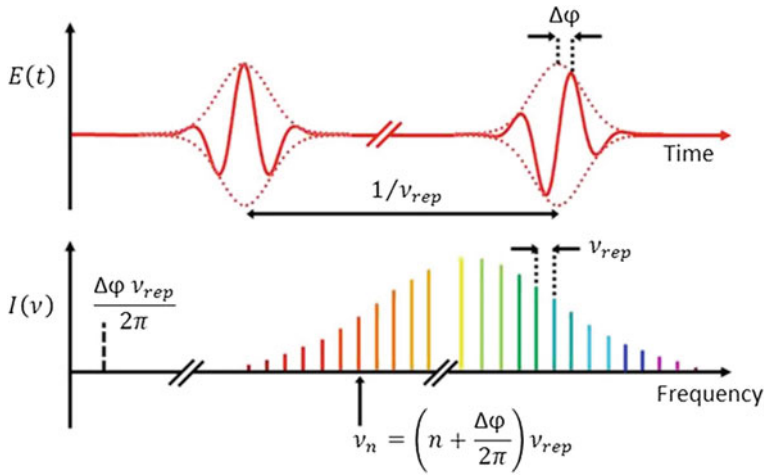

Fig. 11.4 Time (*top*) and frequency (*bottom*) domain representations of an ultrashort pulse train emitted by a femtosecond laser. The spectral width of the frequency comb is inversely proportional to the pulse duration

laser or stabilization of the pulse train emitted by a mode-locked femtosecond laser. Their development in the near-infrared and visible domains has revolutionized optical frequency metrology [46, 49, 50]. Attempts are now being made to extend frequency comb techniques to the mid-infrared spectral region for FTIR and vibrational spectroscopy. Efficient mid-infrared frequency comb generation using ultrafast laser sources promises to significantly expand the variety of possible applications even further [46, 56, 57]. In particular, new spectroscopic and imaging techniques in the "fingerprint region" with dramatically improved precision, sensitivity, recording time and/or spectral bandwidth are being developed which may provide new insights into several unexplored topics in ultrafast biophotonics.

As schematically depicted in Fig. 11.4, the periodic pulse train of a mode-locked femtosecond laser can give rise to a regular comb spectrum of a large number of laser modes with a spacing equal to the pulse repetition frequency [46, 49, 58–60]. Every time the ultrashort pulse circulating in the laser cavity reaches the output coupler, a fraction of its energy is coupled out of the laser. The emitted pulse train therefore has a repetition frequency (ν_{rep}) given by the inverse round-trip time of the pulse in the laser cavity. Due to dispersion in the laser cavity, the carrier wave of the pulse propagates at a phase velocity that differs from the group velocity. Therefore, the electric field of the out-coupled pulses is shifted with respect to the pulse envelope by an amount $\triangle\varphi$ (Fig. 11.4). The Fourier spectrum of the electric field of such a pulse train comprises a series of sharp, equispaced frequency components given by $\nu_n = (n + \frac{\triangle\varphi}{2\pi})\nu_{rep}$, where n is an integer. For applications in precision metrology and spectroscopy, it is mandatory to stabilize $\triangle\varphi$ with high accuracy as any jitter in $\triangle\varphi$ results in broadening of the comb linewidth. There are modelocked

femtosecond lasers which can routinely generate phase stabilized pulse trains with few cycle pulses. Thus commercially available broadband frequency combs have now matured to become standard instruments of precision metrology. The extension of high-sensitivity frequency comb techniques to new spectral regions, from THz frequencies to the extreme-ultraviolet, is likely to open new horizons for advanced diagnostic instruments in biomedicine [46, 49, 58–60]. Several frequency comb generation schemes involving mode-locked lasers, difference frequency generators, optical parametric oscillators, and micro-resonator based Kerr-comb generators have been proposed and demonstrated [46, 56, 57]. The last one in particular also has a small chip-sized footprint and can, therefore, be easily integrated into handheld or portable devices.

Novel techniques have recently been demonstrated in which the frequency comb can be directly used to investigate multiple transitions in an absorbing sample [46, 51, 53, 61–65]. They have been most successfully applied to mid-infrared spectroscopy of gaseous samples which have strong molecular fingerprints but the methods are also promising for liquid and solid samples [66]. These techniques can potentially provide short measurement times ($<1\ \mu s$), high sensitivity (<1 pm), and high accuracy over a broad spectral bandwidth compared to conventional spectroscopy [64]. Experimentally, the frequency comb is selectively attenuated and phase-shifted by molecular resonances; analysis of the latter relies on well-established Fourier transform spectroscopy. The spectroscopic signal is recorded by a single photodetector, overcoming the limitations of dispersive-element based spectrometers [46, 67]. Two different implementations of Fourier transform spectrometers have been reported: Michelson-based Fourier transform spectroscopy, and dual-comb spectroscopy. Each has its own distinct advantages, but both rely on the down-conversion of the high comb frequency signal to a lower frequency range that can be electronically processed. Both schemes are an example of a time-domain technique in which the pulse train of a comb is interferometrically sampled—like in a sampling oscilloscope—by a second pulse train of different repetition frequency [46, 67]. The two schemes shown in Fig. 11.5 differ in the technique used for generating the second pulse train: a Michelson interferometer (Fig. 11.5a) or a second synchronized frequency comb source (Fig. 11.5b). The two interfering frequency combs exiting the interferometer pass the absorbing sample and beat on a photodetector to generate a time-varying low frequency signal [46, 67].

Michelson-based Fourier transform spectroscopy employing an incoherent or coherent broadband source is a well-established technique [46–48]. Therefore, replacing the traditional light source with a frequency comb is not difficult. Dual-comb spectroscopy, in contrast, has only recently been introduced and its full potential is yet to be explored. Use of a mid-infrared frequency comb dramatically reduces measurement time and improves signal-to-noise ratio, even in single-shot measurements, owing to the high spectral radiance of such a coherent source. The sensitivity may be further enhanced by increasing the path length—perhaps by employing a multipass cell or a high-finesse resonator [46, 51, 53, 61–65]. Extremely high sensitivity (one part per billion) has been demonstrated using Michelson based mid-infrared comb FTIR spectroscopy of H_2O_2 [46, 68]. Another intriguing application explores

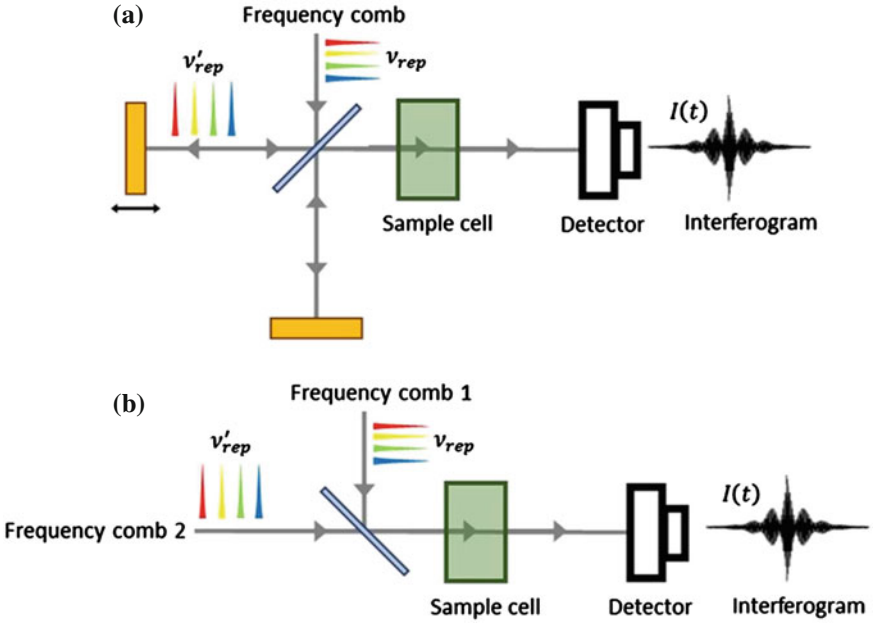

Fig. 11.5 Michelson-based (**a**) and dual-comb (**b**) Fourier transform spectroscopy. Two synchronized pulse trains with slightly different repetition frequencies are mixed to generate a cross-correlation interferogram $I(t)$

combining the potential of broadband near-field microscopy with a frequency comb to interferometrically map the near-field interaction between a metal tip and polar organic molecules [69].

An important practical advantage of a dual comb approach is that being a static scheme, it overcomes shortcomings induced by the moving mirror of the Michelson interferometer; shorter measurement times are the result [46, 52, 55], with spectral resolution being limited only by the measurement time and the intrinsic comb linewidth. The lack of efficient mid-infrared frequency comb sources and the difficulty associated with synchronizing the pulse trains of two combs with interferometric precision have hindered development of this technique. However, an exceptionally high spectral resolution of 12 GHz within a measurement time as low as 10 μs has been demonstrated in proof-of-the-principle experiments [46, 70]. Coherent stimulated Raman dual-comb (imaging) spectroscopy is an alternative technique for accessing fundamental transitions with near-infrared combs [71]. As was done for Michelson based techniques, dual comb based scanning near-field optical microscopy have also been explored [72]. Like in the case of conventional spectroscopy, the spectral range in frequency comb spectrometers is also governed by the bandwidth of the source. However, in frequency comb techniques, unlike in the case of dispersive-element based spectroscopy, the resolution and speed are also governed by source parameters [46, 51, 53, 61–65].

Though frequency comb spectroscopy is still in its infancy, combining it with other laser-based tools in nonlinear optics and electronic signal processing may vastly enhance its range and capabilities. One may even envision chip-size comb spectrometers based on microresonators being developed for real-time biomedical applications. Other than precision spectroscopy, frequency combs may also be used for line-by-line pulse shaping [73], to achieve coherent control over molecular vibrational excitations in biomolecules. Traditional pulse shaping techniques rely on optical elements that are either not transparent or exhibit very low diffraction efficiency in this spectral region, limiting the modulation of the time varying electric field. Many other interesting biophotonic applications, like frequency comb optical coherence tomography [46, 74] of cells and tissues are also likely to emerge in the near future.

11.6 Coherent Control of Biomolecules

Coherent control is a technique for controlling dynamical processes by means of a tailored external optical field. It is based on the quantum mechanical principle that upon excitation, a system can be found in a state that is a superposition of two or more states. The aim here, as schematically depicted in Fig. 11.6, is to steer quantum superposition or interference of the initial states to a specific target state via an appropriately chosen optical field [75–77]. Generally, the light field has to be "shaped" to yield the desired time-dependent spectrum, along with time-dependent phase and polarization to implement coherent control. As ultrashort pulses have a broad spectrum, they permit a wide range of possibilities. The simplest shaped pulse is a chirped pulse, with a time varying frequency (Chap. 2). Accordingly, strong chirp

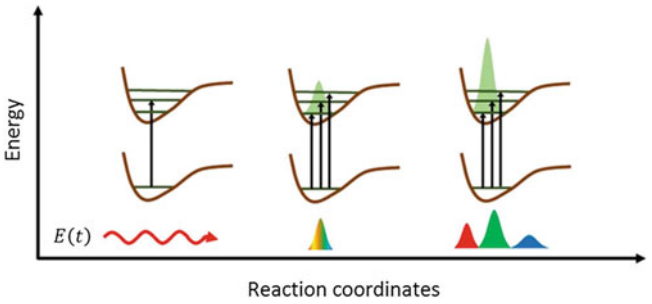

Fig. 11.6 Schematic representation of coherent control. *Left* A cw excitation generally excites only a single vibronic state of the system. *Middle* A transform-limited short pulse excitation results in simultaneous excitation of several vibronic states. The quantum interference between these states generates a wavepacket. *Right* A shaped- or chirped-pulse comprising frequency components with time-varying amplitudes, phase and polarization selectively excites vibronic levels sequentially, each with different efficiency. Such a mechanism affects the interference among several pathways, resulting in enhanced outcome for a particular channel. Thus, proper optimization of the pulse sequence enables control of the photoreaction in a coherent fashion

dependence has been demonstrated in several light-matter interactions like ionization [78, 79], high harmonic generation [80] and nonlinear Raman spectroscopy [81]. Along with a shaped pulse, the technique also needs an automatic feedback control to optimize the yield of the target state [82]. Efficient pulse shaping techniques based on spatial light modulators [83, 84] and optimization control routines involving evolutionary algorithms have been developed [85, 86]. The computational task of finding a control field for a particular target state is difficult and becomes even more difficult with increase in the size of the system. Therefore, it is often possible to control only the outcome of a given chemical reaction, usually involving a specific molecule. In spite of complexity imposed limitations, the technique has diversified, being used in spectroscopy [87–89], quantum information processing [90], laser cooling [91, 92], and plasmonics [93]. The questions to be addressed here are: can coherent control be implemented on photoreactions that are relevant to ultrafast biophotonics? Is it possible to steer biologically important reactions by designing the temporal structure of an optical field?

A photoreaction, similar to that occurring during photosynthesis or vision (Chaps. 7 and 8), involves multiple initial states and can lead to more than one product state. Since these photoreactions are triggered by sunlight or light from incoherent sources, they cannot be steered by the temporal structure of the incident light field. Also, in complex protein molecules, random fluctuations among the enormous number of degrees of freedom might be expected to cancel any interference effects. At the same time, as we have seen in Chaps. 7–9, proteins are highly evolved structures. Indeed, nature steers relevant photoreactions into the desired final states by employing coherent superposition of the protein states as well as those of the surroundings. The quantum interference between multiple pathways in biological systems yields very high efficiency and adaptivity. In the context of "externally-shaped-excitations", coherent control might not be considered to be applicable to biological systems in physiological surroundings. However, its implementation, particularly on a single-molecule level (Chap. 4) could be used as a tool to gain deeper insight into coherent processes in ultrafast biophotonics. It might also help in designing adaptive artificial systems with high efficiencies by blocking unwanted transitions as in biological systems.

An alternate test of quantum coherence in ultrafast biophotonics—other than real-time observation of coherent oscillations using ultrafast 2D spectroscopy or electron microscopy (Chaps. 3, 4 and 7)—is to photoactivate and manipulate biological processes by shaped excitation pulses. Use of ultrafast pulses is mandatory because control can only be achieved on a timescale that is much faster than random thermal motions ($\leq$1 ps), which scramble phase relationships and cause decoherence. The first experiment that used shaped excitation on a biological chromophore involved chirped excitation of the green fluorescent protein (GFP), where adapting the linear chirp to the wavepacket motion in the excited state induced a dynamic Stokes shift [94]. Later, using feedback optimized coherent control of energy flow pathways in the light-harvesting antenna complex LH2 of a photosynthetic purple bacterium, successful steering of $\sim$30 % of the excitation energy into one of the two available product channels was achieved [95]. It is the efficient Raman scattering of

chromophores [96] that accounts for the relatively easy convergence of optimization routines and, consequently, the simplified control.

Which other biological systems or biomolecules are promising candidates for coherent control experiments? Of course, all biological proteins and DNA are potential candidates because of the relevance of their folding processes and technological implications like molecular electronics (Chap. 10). Optical control of the simple photochemical reaction responsible for the primary step of photoisomerization of the retinal molecule in bacteriorhodopsin from the all-*trans* to the 13-*cis* state is another example of the application of coherent control in ultrafast biophotonics [97]. It was demonstrated under weak field conditions (where only 1 of 300 retinal molecules absorbs a photon during the excitation cycle) that are relevant to understanding biological processes. By modulating the phases and amplitudes of the spectral components in the photoexcitation pulse, it was shown that the absolute quantity of the 13-*cis* component formed upon excitation could be enhanced or suppressed by $\sim$20 % of the yield observed using a short transform-limited excitation pulse having the same energy. The observations suggested that the shaped-excitation steered the isomerization through interference effects, a mechanism supported by vibrational coherence discussed in Chaps. 4, 7 and 8. A weak field excitation to control the degree of coherence without causing strong perturbation in the biological protein's environment and dynamics is mandatory to understand behaviour under normal functional conditions. Strong field excitation conditions inevitably access higher-lying excited states and substantially perturb the energy landscape through multiphoton processes [95, 97]. Such effects are usually absent under physiological conditions. These issues are important for interpreting the function of proteins in natural surroundings. However, they are irrelevant if the final objective is to enhance a particular reaction outcome. In this context it is apt to point out that strong field control of the optical field variation within a single 2-cycle 800 nm laser pulse (5 fs laser pulses of 10^{15} W cm^{-2} intensity) has been used to selectively break one of the two equivalent bonds in water molecules [98].

11.7 Probing Biology Beyond the Quantum Limit

The sensitivity that can be attained in experiments on biological entities and processes that involve optical visualization and tracking is, of course, ultimately limited by shot noise—an inevitable consequence of the quantization of light. It is, however, becoming obvious that this quantum limit may be circumvented by utilizing optical states with non-classical photon correlations [99]. Non-classically correlated photons, of the type extensively used in physics, for instance in squeezed light experiments [100] and for gravitational wave detection [101], have begun to find utility in several biological contexts, ranging from quantum optical coherence tomography [102] to determining protein concentrations via entangled photons [103]. However, although non-classically correlated photons were used in these (and similar) experiments, the limit imposed by shot noise was still not overcome.

It may, at first sight, be considered unlikely that squeezed light can be of utility in biological environments, the main reason being the use of high numerical aperture lenses (that are the norm in such experiments) used in conjunction with relatively thick biological samples would lead one to assume that the propagating light becomes so distorted that its spatial mode does not match the detection mode. This is one of the constraints that have inhibited the use of squeezed light in biological experiments for a number of years. Recently, they been overcome in elegant fashion [99] by the expedience of a dual-field technique to replace the usual single field acting both as an oscillator and an interrogator of a bio-sample. In this scheme, a Gaussian probe beam interrogates the bio-sample and, thereby, scatters. A second Gaussian beam whose phase is π-shifted, is used to independently define the detection mode. A single photon detector records the resulting interference between these two fields. The utility of this technique for biologically-relevant studies has already been demonstrated [99] with optically trapped yeast cells, *Sacchoromyces cerevisiae*. Intercellular experiments on different cells have established that the thermally-induced motion of lipid granules inside cells are inhibited by a network of actin filaments which cause the cells' thermal motion to be sub-diffusive. In two-field experiments on yeast cells, one optical field was used to optically trap a yeast cell while a second, shaped local oscillator field probed the trapped cells' motion. The parameter that was measured in these experiments was the mean square displacement (MSD) which, for the thermally-induced motion of a free particle, may be expressed as [99]:

$$\Delta x^2(\tau) = \left\langle [x(t) - x(t-\tau)]^2 \right\rangle = 2D\tau^{\alpha}. \tag{11.1}$$

Here, τ is a measure of the time delay between successive measurements and D is the diffusion constant; α is the cell medium's viscoelasticity. In the purely viscous regime, in which each yeast cell will undergo Brownian motion, $\alpha = 1$. The signature of the sub-diffusive regime is when $\alpha < 1$.

Test measurements were conducted on silica beads of a few μm dimension and they yielded a value of α that was unity to all intents and purposes (0.994 ± 0.006) [99]. In measurements conducted on yeast cells, values of α were obtained that ranged from 0.6 to 1.0, depending on which part of the local aqueous environment the lipid particles interacted with. When MSD measurements were made using squeezed light, significantly enhanced precision (by $\sim$22 %) was obtained in comparison with measurements using coherent light, allowing up to 64 % enhancement of measurement rate while, at the same time, maintaining precision. The implication of such experiments is that a significantly better experimental capability appears attainable for making time-dependent measurements of motion in a biological environment. It is certainly looking likely that further use of squeezed light in biological applications will be forthcoming which will enhance the scope of biological phenomena and processes that become amenable to quantitative investigations [104, 105]. As has been shown [103], ultrafast laser science is likely to play an important role in such experiments by permitting microfluidic channels to be laser-written, in materials like fused silica. Writing such microchannels constitutes an extension of well-developed methods of laser-writing of waveguides [106–108], with strong HF acid used to etch

the waveguides into hollow channels through which fluids can flow (mainly by capillary action). Crespi et al. [103] have devised an elegant experimental scheme in which a femtosecond-laser-written microfluidic channel is made to pass through one arm of a conventional Mach-Zehnder interferometer. When a liquid biological sample is fed into the microfluidic channel, the relative phase shift of light that occurs in the sensing arm of the interferometer manifests itself in the interference fringes that are observed.

11.8 Probing Biology on Attosecond Timescales

It has been demonstrated that trains of attosecond (as) pulses as well as isolated pulses of duration as short as ∼70 as can be reliably generated by means of the high-harmonic generation process. Typical photon energies in attosecond pulses range from ∼15–120 eV. Experiments have begun to be conducted that probe dynamics in the attosecond regime, and these have, in the main, used a combination of a single attosecond pulse and a carrier-envelope-phase (CEP) stabilized pulse in the near infrared (∼800 nm wavelength) whose pulse duration is typically ∼5 fs. This, in itself, presents a not-inconsiderable technical challenge in achieving temporal overlap of ultrashort and not-so-ultrashort pulses so as to achieve attosecond time resolution. Initial experiments on atomic systems have yielded intriguing results but their interpretation continues to present challenges. The influence of *two* intense, time-dependent optical fields has to be unravelled, keeping in mind that molecular potential energy surfaces—of even a one-electron molecule like H_2^+—undergo very substantial morphological changes in the course of an intense, 5 fs long, CEP-stabilized pulse [109, 110]. It is certain that attosecond time-resolved experiments on biomolecules will be rewarding once conceptual barriers (like how to properly deal with the inevitable transient distortion of electronic structures in ultrashort pulses of intense optical fields) are surmounted.

Biological entities that are sought to be probed on attosecond timescales will, almost inevitably, be in the condensed phase. As has been noted [111], such experiments will open the possibility of following, with high sensitivity, changes in the oxidation state, chemical environment and electronic state of the atomic and molecular constituents by monitoring the effect that electrons (or holes) have on various sites within the medium. The use of attosecond excitation in such studies will make it possible to record "images" of biochemical processes like charge migration within diverse media of biological significance.

We have already discussed tunneling effects that occur in biological molecules in Chap. 9. Tunneling processes occur on attosecond and femtosecond timescales. There are intriguing possibilities of tunneling effects proving useful for developing new DNA sequencing methodologies. We know that it is the sequence of four bases—adenine (A), guanine (G), thymine (T), and cytosine (C)—that determines genetic information which governs the structure and function of all living entities. It is not unexpected that efforts have already commenced to develop reliable and

easy-to-implement techniques that will help establish the order of bases in DNA. The currently employed methods of such DNA sequencing continue to be complicated and time-consuming: they involve elaborate schemes of optical detection and computer-intensive sequence determination in order that information is obtained on the biochemistry that drives DNA fragmentation, amplification and chain termination. Next generation DNA sequencing (NGS) seeks to improve the throughput of the process, at lower costs [112, 113], but issues connected with errors and an apparent limit on the length of DNA that can be probed [114] continue to be barriers. Perhaps the use of tunnelling DNA sequencing might prove to be useful.

In nanopore sequencing [115–117] single-stranded DNA (in a physiologically-appropriate aqueous solution) is forced through a nanosized pore. As noted, femtosecond laser writing is employed to fabricate such pores. Ion-induced currents are generated as the nucleotides block the nanopore, and such currents can be correlated with the type of base in a given nucleotide. Nanopores used in early studies were made from biological materials [118, 119] but it is likely that graphene nanopores may be of utility in future. Graphene offers the advantage of providing an atomic layer thickness which might permit the attainment of single-base resolution [120–122]. The transverse ion current generated in such nanopores is, of course, due to tunnelling—an ultrafast process. Both the magnitude of the tunnelling current as well as the structural noise that accompanies it, carry signatures of the geometrical alignment of proximate bases. It has been possible to carry out modelling exercises by treating DNA as a large-bandgap amorphous semiconductor (with a π-π bandgap of $\sim$4 eV) [123].

11.9 Future Opportunities Offered by Ultrafast Biophotonics

Biological systems achieve several functionalities—respiration involving electron tunneling, photosynthesis involving quantum coherence, vision and DNA photolyases—with efficiencies that are usually impossible to imagine in artificial systems. As we have seen throughout this book, many, if not all, of these capabilities rely on ultrafast phenomena that occur on nanometric lengthscales and that rely on very precise arrangements of molecules. Of course, as with everything in nature, all such molecular arrangements are achieved through self assembly. Ultrafast biophotonics, along with methods of synthetic biology, offers exciting opportunities to develop deeper understanding of these biological functionalities as well as for making progress in mimicking nature's design principles in artificial devices. Potential areas for developing efficient biomimetic ultrafast devices involve solar energy harvesting, sensing, energy storage, and molecular electronics: many other possibilities await exploration.

References

1. W. Min, B.P. English, G. Luo, B.J. Cherayil, S.C. Kou, X.S. Xie, Acc. Chem. Res. **38**, 923 (2005)
2. D. Brinks, F.D. Stefani, F. Kulzer, R. Hildner, T.H. Taminiau et al., Nature **465**, 905 (2010)
3. R. Henderson, Quart. Rev. Biophys. **28**, 171 (1995)
4. R. Neutze, R. Wout, D. van der Spoel, E. Weckert, J. Hajdu, Nature **406**, 752 (2000)
5. H.N. Chapman, S.P. Hau-Riege, M.J. Bogan, S. Bajt, A. Barty et al., Nature **448**, 676 (2007)
6. H.N. Chapman, P. Fromme, A. Barty, T.A. White, R.A. Kirian et al., Nature **470**, 73 (2011)
7. M.M. Seibert, T. Ekeberg, F.R.N.C. Maia, M. Svenda, J. Andreasson et al., Nature **470**, 78 (2011)
8. B. La Scola, S. Audic, C. Robert, L. Jungang, X. de Lamballerie et al., Science **299**, 2033 (2003)
9. M.R. Sawaya, D. Cascio, M. Gingery, J. Rodriguez, L. Goldschmidt et al., Proc. Nat. Acad. Sci. **111**, 12769 (2014)
10. R. Koopmann, K. Cupelli, L. Redecke, K. Nass, D.P. Deponte et al., Nat. Methods **9**, 259 (2012)
11. Y. Takayama, S. Maki-Yonekura, T. Oroguchi, M. Nakasako, K. Yonekura, Sci. Rep. **5**, 08074 (2015)
12. M. Nakasako, Y. Takayama, T. Oriquichi, Y. Sekiquchi, A. Kobayashi et al., Rev. Sci. Instrum. **84**, 093705 (2013)
13. C. Rischel, A. Rousse, I. Uschmann, P.-A. Albouy, J.-P. Geindre et al., Nature **390**, 490 (1997)
14. J. Miao, P. Charalambous, J. Kirz, D. Sayre, Nature **400**, 342 (1999)
15. H. Ihee, V.A. Lobastov, U.M. Gomez, B.M. Goodson, R. Srinivasan et al., Science **291**, 458 (2001)
16. J.C.H. Spence, R.B. Doak, Phys. Rev. Lett. **92**, 198102 (2004)
17. W.E. Moerner, M. Orrit, Science **283**, 1670 (1999)
18. S. Weiss, Science **283**, 1676 (1999)
19. Y.C. Sasaki, Y. Okumura, S. Adachi, H. Suda, Y. Taniguchi, N. Yagi, Phys. Rev. Lett. **87**, 248102 (2001)
20. N. Ogawa, K. Hoshisashi, H. Sekiguchi, K. Ichiyanagi, Y. Matsushita et al., Sci Rep. **3**, 2201 (2013)
21. R.S. Mathew-Fenn, R. Das, P.A.B. Harbury, Science **322**, 446 (2008)
22. R.S. Mathew-Fenn, R. Das, J.A. Silverman, P.A. Walker, P.A.B. Harbury, PLoS One **3**, e3229 (2008)
23. X. Shi, D. Herschlag, P.A.B. Harbury, Proc. Natl. Acad. Sci. USA **110**, E1444 (2013)
24. D. Sayre, Acta Crystallogr. **5**, 843 (1952)
25. Y. Nishino, Y. Takahashi, N. Imamoto, T. Ishikawa, K. Maeshima, Phys. Rev. Lett. **102**, 018101 (2009)
26. M.A. Pfeifer, G.J. Williams, I.A. Vartanyants, R. Harder, I.K. Robinson, Nature **442**, 63 (2006)
27. J.R. McIntosh, *Cellular Electron Microscopy, Methods in Cell Biology* (Academic Press, San Diego, 2007)
28. J. Kirz, C. Jacobsen, M. Howells, Quart. Rev. Biophys. **28**, 33 (1995)
29. W. Chao, B.D. Harteneck, J.A. Liddle, E.H. Anderson, D.T. Attwood, Nature **435**, 1210 (2005)
30. J.R. Fienup, Appl. Opt. **21**, 2758 (1982)
31. M. Germann, T. Latychevskaia, C. Escher, H.-W. Fink, Phys. Rev. Lett. **104**, 095501 (2010)
32. M. Hoshino, K. Uesugi, N. Yagi, S. Mohri, J. Regini, B. Pierscionek, PLoS One **6**, e25140 (2011)
33. A. Momose, S. Kawamoto, I. Koyama, Y. Hamaishi, K. Takai, Y. Suzuki, Jpn. J. Appl. Phys. **42**, L866 (2003)
34. A. Momose, Jpn. J. Appl. Phys. **44**, 6355 (2005)
35. J. Wang, Nucleic Acids Res. **28**, 3011 (2000)
36. M.L. Larramendy, W. El-Rifai, S. Knuutila, Cytometry **31**, 174 (1998)

37. Z. Zhu, A.S. Waggoner, Cytometry **28**, 206 (1997)
38. X.C. Zhang, Phys. Med. Biol. **47**, 3667 (2002)
39. W. Zhang, E.R. Brown, M. Rahman, M.L. Norton, Appl. Phys. Lett. **102**, 023701 (2013)
40. T.R. Globus, D.L. Woolard, T. Khromova, T.W. Crowe, M. Bykhovskaia et al., J. Biol. Phys. **29**, 89 (2003)
41. A. Markelz, S. Whitmire, J. Hillebrecht, R. Birge, Phys. Med. Biol. **47**, 3797 (2002)
42. R.M. Woodward, V.P. Wallace, D.D. Arnone, E.H. Linfield, M. Pepper, J. Biol. Phys. **29**, 257 (2003)
43. S.E. Whitmire, D. Wolpert, A.G. Markelz, J.R. Hillebrecht, J. Galan, R.R. Birge, Biophys. J. **85**, 1269 (2003)
44. C.F. Zhang, E. Tarhan, A.K. Ramdas, A.M. Weiner, S.M. Durbin, J. Phys. Chem. B **108**, 10077 (2004)
45. M. Tang, Q. Huang, D. Wei, G. Zhao, T. Chang et al., J. Biomed. Opt. **20**, 095009 (2015)
46. A. Schliesser, N. Picqué, T.W. Hänsch, Nature Photon. **6**, 440 (2012)
47. Z. Movasaghi, S. Rehman, I. ur Rehman, Appl. Spectrosc. Rev. **43**, 134 (2008)
48. D.I. Ellis, R. Goodacre, Analyst **131**, 875 (2006)
49. T.W. Hänsch, Rev. Mod. Phys. **78**, 1297 (2006)
50. A. Schliesser, M. Brehm, F. Keilmann, D.W. van der Weide, Opt. Exp. **13**, 9029 (2005)
51. S.A. Diddams, L. Hollberg, V. Mbele, Nature **445**, 627 (2007)
52. I. Coddington, W.C. Swann, N.R. Newbury, Phys. Rev. Lett. **100**, 013902 (2008)
53. J. Mandon, G. Guelachvili, N. Picqué, Nature Photon. **3**, 99 (2009)
54. A. Foltynowicz, P. Masłowski, T. Ban, F. Adler, K.C. Cossel et al., Faraday Discuss. **150**, 23 (2011)
55. A.M. Zolot, F.R. Giorgetta, E. Baumann, J.W. Nicholson, W.C. Swann et al., Opt. Lett. **37**, 638 (2012)
56. A.A. Savchenkov, A.B. Matsko, D. Strekalov, M. Mohageg, V.S. Ilchenko, L. Maleki, Phys. Rev. Lett. **93**, 243905 (2004)
57. P. Del'Haye, A. Schliesser, O. Arcizet, T. Wilken, R. Holzwarth, T.J. Kippenberg, Nature **450**, 1214 (2007)
58. T. Udem, R. Holzwarth, T.W. Hänsch, Nature **416**, 233 (2002)
59. S.T. Cundiff, J. Ye, Rev. Mod. Phys. **75**, 325 (2003)
60. S.T. Cundiff, J. Ye, *Femtosecond Optical Frequency Comb: Principle, Operation and Applications* (Springer, New York, 2005)
61. B. Bernhardt, A. Ozawa, P. Jacquet, M. Jacquey, Y. Kobayashi et al., Nature Photon. **4**, 55 (2010)
62. M.J. Thorpe, K.D. Moll, R. Jason, Jones, B. Safdi, J. Ye, Science **311**, 1595 (2006)
63. M.J. Thorpe, J. Ye, Appl. Phys. B **91**, 397 (2008)
64. Y. Bao, X. Yi, Z. Li, Q. Chen, J. Li, X. Fan, X. Zhang, Light Sci. Appl. **4**, e300 (2015)
65. G. Millot, S. Pitois, M. Yan, T. Hovhannisyan, A. Bendahmane et al., Nature Photon. **10**, 27 (2016)
66. T. Ganz, M. Brehm, H.G. von Ribbeck, D.W. van der Weide, F. Keilmann, New J. Phys. **10**, 123007 (2008)
67. P.R. Griffiths, J.A. De Haseth, *Fourier Transform Infrared Spectroscopy*, 2nd edn. (Wiley, New York, 2007)
68. A. Foltynowicz, P. Maslowski, A.J. Fleisher, B.J. Bjork, J. Ye, App. Phys. B **110**, 163 (2013)
69. S. Amarie, F. Keilmann, Phys. Rev. B **83**, 045404 (2011)
70. E. Baumann, F.R. Giorgetta, W.C. Swann, A.M. Zolot, I. Coddington, N.R. Newbury, Phys. Rev. A **84**, 062513 (2011)
71. T. Ideguchi, S. Holzner, B. Bernhardt, G. Guelachvili, N. Picqué, T.W. Hänsch, Nature **502**, 355 (2013)
72. M. Brehm, A. Schliesser, F. Keilmann, Opt. Express **14**, 11222 (2006)
73. S.T. Cundiff, A.M. Weiner, Nature Photon. **4**, 760 (2010)
74. S.J. Lee, B. Widiyatmoko, M. Kourogi, M. Ohtsu, Jpn. J. Appl. Phys. **40**, L878 (2001)
75. D.J. David, S.A. Rice, J. Chem. Phys. **83**, 5013 (1985)

76. P. Brumer, M. Shapiro, Chem. Phys. Lett. **126**, 541 (1986)
77. R.J. Gordon, S.A. Rice, Ann. Rev. Phys. Chem. **48**, 601 (1997)
78. D. Mathur, F.A. Rajgara, J. Chem. Phys. **120**, 5616 (2004)
79. D. Mathur, K. Dota, A.K. Dharmadhikari, J.A. Dharmadhikari, Phys. Rev. Lett. **110**, 083602 (2013)
80. R. Bartels, S. Backus, E. Zeek, L. Misoguti, G. Vdovin et al., Nature **406**, 164 (2000)
81. N. Dudovich, D. Oron, Y. Silberberg, Nature **418**, 512 (2002)
82. R.S. Judson, H. Rabitz, Phys. Rev. Lett. **68**, 1500 (1992)
83. A.M. Weiner, Rev. Sci. Instrum. **71**, 1929 (2000)
84. K. Hitoshi, M.M. Wefers, K.A. Nelson, Annu. Rev. Phys. Chem. **46**, 627 (1995)
85. A. Assion, T. Baumert, M. Bergt, T. Brixner, B. Kiefer et al., Science **282**, 919 (1998)
86. B. Constantin, R. Chakrabarti, H. Rabitz, New J. Phys. **12**, 075008 (2010)
87. M. Dantus, V.V. Lozovoy, Chem. Rev. **104**, 1813 (2004)
88. D. Meshulach, Y. Silberberg, Nature **396**, 239 (1998)
89. Y. Silberberg, Annu. Rev. Phys. Chem. **60**, 277 (2009)
90. E. Knill, R. Laflamme, R. Martinez, C.-H. Tseng, Nature **404**, 368 (2000)
91. M. Viteau, A. Chotia, M. Allegrini, N. Bouloufa, O. Dulieu et al., Science **321**, 232 (2008)
92. C.-Y. Lien, C.M. Seck, Y.-W. Lin, J.H.V. Nguyen, D.A. Tabor, B.C. Odom, Nat. Commun. **5**, 4783 (2014)
93. M. Aeschlimann, T. Brixner, A. Fischer, C. Kramer, P. Melchior et al., Science **333**, 1723 (2011)
94. C.J. Bardeen, V.V. Yakovlev, J.A. Squier, K.R. Wilson, J. Am. Chem. Soc. **120**, 13023 (1998)
95. W. Wohlleben, T. Buckup, J.L. Herek, M. Motzkus, Chem. Phys. Chem **6**, 850 (2005)
96. H.A. Frank, A.J. Young, G. Britton, R.J. Cogdell, *The Photochemistry of Carotenoids* (Kluwer, Dordrecht, 1999)
97. V.I. Prokhorenko, A.M. Nagy, S.A. Waschuk, L.S. Brown, R.R. Birge, R.J.D. Miller, Science **313**, 1257 (2006)
98. D. Mathur, K. Dota, D. Dey, A.K. Tiwari, J.A. Dharmadhikari et al., J. Chem. Phys. **143**, 244310 (2015)
99. M.A. Taylor, J. Janousek, V. Daria, J. Knittel, B. Hage et al., Nature Photon. **7**, 229 (2013)
100. F. Wolfgramme, A. Cerè, F.A. Beduini, A. Predojević, M. Koschorreck, M.W. Mitchell, Phys. Rev. Lett. **105**, 053601 (2010)
101. J. Abadie et al., the LIGO Scientific Collaboration. Nature Phys. **7**, 962 (2011)
102. M.B. Nasr, D.P. Goode, N. Nguyen, G. Rong, L. Yang, B.M. Reinhard, B.E.A. Saleh, M.C. Teich, Opt. Commun. **282**, 1154 (2011)
103. A. Crespi, M. Lobino, J.C.F. Matthews, A. Politi, C.R. Neal et al., Appl. Phys. Lett. **100**, 233704 (2012)
104. G. Brida, M. Genovese, I.R. Berchera, Nature Photon. **4**, 227 (2010)
105. V. Giovannetti, S. Lloyd, L. Maccone, Science **306**, 1330 (2004)
106. P. Nandi, G. Jose, C. Jayakrishnan, S. Debbarma, K. Chalapathi et al., Opt. Express **14**, 12145 (2006)
107. J.A. Dharmadhikari, K. Pradyna, A. Bhatnagar, D. Mathur, A.K. Dharmadhikari, Opt. Commun. **287**, 122 (2013)
108. J.A. Dharmadhikari, R. Bernard, A.K. Bhatnagar, D. Mathur, A.K. Dharmadhikari, Opt. Lett. **38**, 172 (2013)
109. M. Garg, A.K. Tiwari, D. Mathur, J. Phys. Chem. A **116**, 8762 (2012)
110. D. Mathur, A.K. Tiwari, in *Concepts and Methods in Modern Theoretical Chemistry*, vol. 2, S. K. Ghosh, P. Chattaraj (Eds.) (Taylor and Francis, Boca Raton, 2013)
111. S.R. Leone, C.W. McCurdy, J. Burgdörfer, L.S. Cederbaum, Z. Chang et al., Nature Photon. **8**, 162 (2014)
112. J. Shendure, H. Ji, Nature Biotechnol. **26**, 1135 (2008)
113. M.L. Metzker, Nat. Rev. Genet. **11**, 31 (2009)
114. C.W. Fuller, L.R. Middendorf, S.A. Benner, G.M. Church, T. Harris et al., Nature Biotechnol. **27**, 1013 (2009)

115. M. Di Ventra, Nanotechnology **24**, 342501 (2013)
116. R.H. Scheicher, A. Grigoriev, R. Ahuja, J. Mater. Sci. **47**, 7439 (2012)
117. B.M. Venkatesan, R. Bashir, Nature Nanotech. **6**, 615 (2011)
118. J.J. Kasianowicz, E. Brandin, D. Branton, D.W. Deamer, Proc. Natl. Acad. Sci. USA **93**, 13770 (1996)
119. J. Li, D. Stein, C. McMullan, D. Branton, M.J. Aziz, J.A. Golovchenko, Nature **412**, 166 (2001)
120. K.K. Saha, M. Drndić, B.K. Nikolić, Nano Lett. **12**, 50 (2012)
121. T. Nelson, B. Zhang, O.V. Prezhdo, Nano Lett. **10**, 3237 (2010)
122. H.W.C. Postma, Nano Lett. **10**, 420 (2010)
123. J.R. Alvarez, D. Skachkov, S.E. Massey, J. Lu, A. Kalitsov, J.P. Velev, Phys. Rev. Appl. **1**, 034001 (2014)